2H-MoS$_2$ as an Artificial Solid Electrolyte Interface in All-Solid-State Lithium–Sulfur Batteries

Abdulkadir Kızılaslan,* Tuğrul Çetinkaya, and Hatem Akbulut

All-solid-state lithium-ion batteries are considered the next-generation energy storage systems. However, certain problems arise from the degradation of anode–electrolyte interface hindering their use especially when lithium is used as an anode. Herein, lithium metal anode surface is modified by an artificial 2H-MoS$_2$ layer to prevent the contact between highly reactive lithium and solid electrolyte without sacrificing the lithium ion transport. The stabilization of the electrode/electrolyte interface is attributed to the electrochemical stability of the 2H-MoS$_2$ layer. Besides, high ionic conductivity and selective sieving nature of layered MoS$_2$ neither prevents the electrochemical reactions nor increases the total impedance of the cell. Electrochemical stability of the electrode/electrolyte interface is shown by long-term chronoamperometry and chronovoltammetry tests. By stabilizing electrode/electrolyte interface, initial and final discharge capacities of 675.8 and 584.1 mAh g^{-1}, respectively, is obtained at 0.4 mA cm^{-2} current density in MoS$_2$@Li/ Li$_7$P$_3$S$_{11}$/S. After 200 cycles, discharge capacity fade is obtained as 13.58% and 27.3% for the cells assembled with MoS$_2$@Li and bare Li anodes, respectively.

1. Introduction

The use of fossil fuels and accompanied environmental problems triggered the scientific studies to build new energy storage systems. Lithium-ion batteries (LIBs) are considered the most prominent alternatives to replace the use of fossil fuels on vehicles. As we approach to the theoretical capacity limits of LIBs, lithium–sulfur batteries emerged as new potential energy storage system with their theoretical energy density of 2500 Wh kg^{-1}.[1–3]

Dr. A. Kızılaslan, Dr. T. Çetinkaya, Prof. H. Akbulut
Metallurgy and Materials Science Department
Sakarya University
Esentepe Campus, Sakarya 54187, Turkey
E-mail: akizilaslan@sakarya.edu.tr
Dr. A. Kızılaslan, Dr. T. Çetinkaya, Prof. H. Akbulut
Development and Application Center (SARGEM)
Sakarya University
Esentepe Campus, Sakarya 54187, Turkey
Dr. T. Çetinkaya, Prof. H. Akbulut
NESSTEC Energy & Surface Technology A.S.
Technology Development Zones
Sakarya University
Sakarya, Turkey

Regardless of the battery type, Li-ion (sulfur) or Li-O$_2$, it is rational to consider the lithium metal as the anode material in these batteries due to several aspects. First, it is the lightest solid (0.534 g cm^{-3}) in the whole periodic table and has the lowest electrode potential with −3.04 V.[4,5] Second, as a pure lithium source, an intercalation or conversion reaction media is not necessarily required in batteries with lithium anodes. Overall, lithium metal has a theoretical specific capacity of ≈3860 mAh g^{-1}.[4] However, many problems arising from the highly reactive nature of lithium metals, namely; 1) uncontrollable dendrite formation during lithium deposition\dissolution and 2) unstable solid-electrolyte interface (SEI) layer formation, restricts its use in secondary batteries.

All-solid-state LIBs (ASSLIBs) are now emerging systems to replace LIBs with liquid electrolytes and are free of the aforementioned problems in certain aspects. Solid-electrolytes were shown to greatly suppress the formation of lithium dendrites. However, the formation of an unstable SEI layer still exists in ASSLIBs. Although solid electrolytes with lithium-ion conductivity on the order of liquid electrolytes have been synthesized,[6–9] their adaption into a cell with lithium anode is hindered due to the formation of unstable SEI layer. A stable SEI layer has to meet several criteria. First, an SEI layer has to be composed of electronically (ionically) insulating (conducting) phases. Besides, the layer should be thin and dense enough so that the total impedance of the system does not increase due to the low ionic conductivity of the layer.

Unfortunately, only a few numbers of solid electrolytes exist that satisfies the above mentioned criteria. One plausible way to avoid the self-formation of the unstable SEI layer is to coat the lithium anode with the phases having desired properties. By coating lithium anode; 1) the contact between anode and electrolyte can be increased due to better wetting, 2) dendrite formation can be eliminated, and 3) electrolyte decomposition can be prevented. Li$_3$N coating was shown to increase capacity retention in our previous study.[10] However, the small grain sizes (<160 nm), and weak interconnection is not capable of suppressing Li metal dendrites for long cycles.[11] Moreover, the voltage stability window of Li$_3$N is only ≈0.45 V and unstable to reduction (≤2.4 V vs Li/Li$^+$) which is low for practical applications.[12] An ultrathin Al$_2$O$_3$ layer was shown to increase the wetting and electrochemical stability of the garnet-type solid

**ADVANCED
SCIENCE NEWS**

www.advancedsciencenews.com

**ADVANCED
MATERIALS
INTERFACES**

www.advmatinterfaces.de

electrolyte.[13,14] Similarly, a thin LiPON layer on lithium anode effectively prevented the formation of lithium dendrites even at high currents.[15]

2D materials, especially transition metal dichalcogenides (TMDCs) are attractive materials in the synthesis of advanced functional materials.[16–19] Among TMDCs, molybdenum disulfide (MoS_2) has attracted much interest in recent studies as an anode material for LIBs to replace graphite anode due to the high capacity of 670 mAh g^{-1}.[20–23] Besides, MoS_2 and its derivatives are utilized in different forms of energy storage systems.[24–26] As similar to graphite, MoS_2 has a layered structure of covalently bonded Mo—S—Mo units into a hexagonal lattice. The large interlayer distance of 0.62 nm (0.34 nm in graphite) facilitates the fast lithium ion diffusion in the structure.[27,28] Moreover, theoretical studies reveal that unlike graphene where lithium ions strongly bind to defects, lithium ions loosely adsorb onto MoS_2 defects and lithium-ion diffusion does not hinder.[29–31] The diffusion energy barrier was calculated in the range of 0.21–0.29 eV in different studies[32,33] and Shuai et al. showed that the diffusion kinetics of MoS_2 can be controlled by the adjustment of its layer spacing.[34] As a challenge to utilize MoS_2 as an anode in LIBs, MoS_2 is a poor electrical conductive material. In fact, many studies were focused on to increase the conductivity of MoS_2.[35–37] However, as an artificial SEI layer, the poor electronic conductivity of MoS_2 is an asset once sufficient ionic conductivity ensured thorough adjusting the thickness of the layer. MoS_2 is also utilized as lithium ion conductive membrane in LIBs with liquid electrolytes, thanks to their selective ion transport characteristics.[38–41] Recently, Cha et al. have utilized 10 nm thick 2D MoS_2 as a protective layer for lithium metal anodes in liquid based lithium sulfur batteries and reported that MoS_2 provides good adhesion on the surface of lithium metal and enhance the Li^+ transport and conductivity.[42] Similarly, Yao et.al.[43] used bilayer solid electrolyte to avoid the reaction between the highly reactive lithium anode and solid electrolyte. Although many attempts to utilize protective layers in LIBs with liquid electrolyte systems have been carried out, the analysis of such layers in ASSLIBs is still in its infancy. Besides, studies reported in the literature are utilized thin film coating techniques that are hard to be scaled up for mass production and not cost effective.

In this study, we report a facile coating of MoS_2 onto lithium anode as an artificial SEI layer in ASSLIBs and evaluation of the electrochemical performance of the cells assembled with bare and MoS_2 coated lithium. By utilizing the selective sieving and highly stable nature of MoS_2, the layer is expected to prevent the degradation of solid electrolyte and corrosion of lithium anode through preventing the contact between the anode and solid electrolyte. Highly ionic conductive $Li_7P_3S_{11}$ and sulfur based composite cathode were utilized as solid electrolyte and cathode, respectively in this study.

2. Results and Discussion

The phase analysis of the coating on the lithium surface was performed using XRD analysis. **Figure 1**a displays the XRD analysis result of the coating layer. The layer crystallizes in 2H-MoS_2 with a highly crystalline nature in $P6_3/mmc$ [194]

symmetry where the atomic structure of the phase is given in Figure 1b,c. The structure has one layer of Mo that is sandwiched between two layers of S which is known as the most stable polymorph of MoS_2 phases. The layers are connected to each other thorough weak Van der Waals interactions and expected to supply paths for lithium ion diffusion. The distance between the layers (0.62 nm) is approximately twice as much as the distance in graphite so that lithium ion movement between the layers is expected to be much easier compared to graphite. Low and high magnification field emission scanning electron microscope (FESEM) image of exfoliated 2H-MoS_2 is shown in Figure 1d,e. It is obvious that MoS_2 structure was exfoliated successfully and flake size was altered between 1 and 4 µm.

Structural analysis of MoS_2 layer on lithium anode was carried out by FESEM, and the corresponding cross section images are given in **Figure 2**a,b at low and high magnifications with a 5° tilt angle. A thin layer of MoS_2 is observed on the surface. Oxides are formed on the cross section due to the transfer of lithium chip from the glovebox to the chamber of electron microscopy. The homogeneous distribution of the MoS_2 layer on lithium chip is also shown at higher magnification in Figure 2b where the oxides are more obvious in the cross section.

Figure 2c displays the surface of the lithium chip partially coated with MoS_2 layer. The thickness of the coating layer was measured as 2.0 µm. Considering the overall impedance of the cell, the coating layer has to be thin and uniform to prevent local impedance arising due to the uneven coating. In fact, unlike LIBs with liquid electrolytes, extremely thin layers formed by thin film coating techniques is hard to be utilized in ASSLIBs due to their vulnerability under the operating pressure of these cells.

Figure 3 displays the cyclic voltammetry (CV) curves of the asymmetric Li/$Li_7P_3S_{11}$/stainless steel (SUS) and MoS_2@Li/$Li_7P_3S_{11}$/SUS cells in the potential range of −0.5–5 V (vs Li/Li^+). A wide electrochemical window of 5 V was measured in both cells with lithium ion stripping and deposition reactions observed at 0.27 V and just below 0 V, respectively. No reaction was detected between MoS_2 and Li during the anodic and cathodic sweep, attributed to the stable interface behavior of 2D MoS_2. However, a close look at the CV curves indicates that there is a large fluctuation in the current in bare-lithium compared to MoS_2@Li. Such fluctuations in the current demonstrate that the compatibility between lithium and solid electrolyte was increased by MoS_2 coating. Such small fluctuations in the current would inevitably deteriorate the stability between electrode and electrolyte in long cycles.[44] So that batteries expected to operate long times have to be constructed with elements having stable interfaces.

In fact, electrochemical window analyses conducted by CV tests can just barely catch the reactions that stands for the degradation of the interfaces due to the fast scan rates.[45] Therefore, in order to check the stability of the electrode/electrolyte interface, we have constructed symmetric Li/$Li_7P_3S_{11}$/Li and MoS_2@Li/$Li_7P_3S_{11}$/MoS_2@Li cells. Long term chronoamperometry scan at different voltages was carried out. **Figure 4**a displays the long time span current response of the symmetric cells at a constant voltage. Fade in the current over time is attributed to the incompatibility in the electrode/electrolyte interface. In fact,
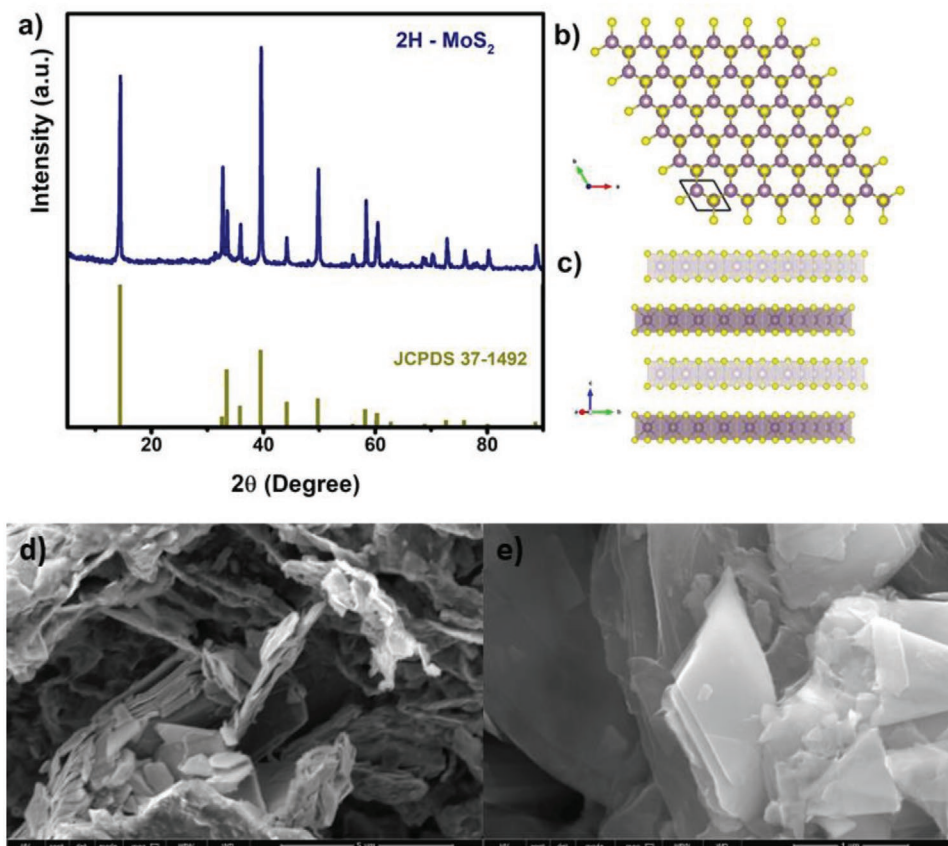
**ADVANCED
SCIENCE NEWS**

www.advancedsciencenews.com

**ADVANCED
MATERIALS
INTERFACES**

www.advmatinterfaces.de

Figure 1. a) XRD analysis of exfoliated 2H-MoS$_2$, b) basal plane view, c) *c*-axis view of 2H-MoS$_2$ crystal structure (sulfur and molybdenum are depicted in yellow and blue colors, respectively), d) low, and e) high magnification SEM images of exfoliated 2H-MoS$_2$ layers.

Wenzel et al. characterized the interface where the formation of Li$_2$S and P$_2$S$_5$ due to the degradation of Li$_7$P$_3$S$_{11}$ was shown by XPS analysis.[46] In Li$_2$S-P$_2$S$_5$-MS$_2$ (M: Ge, Sn, and Si) systems, this phenomenon is even more severe due to the reduction of solid electrolyte in contact with lithium anode.[47] However, in MoS$_2$@Li current response to the applied voltage even at 30 and 50 mV is stable over a longer time span which testifies the compatibility between the interfaces Li/MoS$_2$ and MoS$_2$/Li$_7$P$_3$S$_{11}$. Steady-state current at 0.01 V is higher in MoS$_2$ coated system, which is attributed to less resistance for Li depositing and stripping at the interface.[48]

The compatibility between the electrode/electrolyte interface was further demonstrated by chronovoltammetry analysis at increasing current densities as shown in Figure 4b. Symmetric Li/Li$_7$P$_3$S$_{11}$/Li and MoS$_2$@Li/Li$_7$P$_3$S$_{11}$/MoS$_2$@Li cells were repeatedly charged and discharged at different current densities. The polarization voltage of bare lithium is higher compared to MoS$_2$@Li which shows the incompatibility of Li/Li$_7$P$_3$S$_{11}$ interface.[49] However, in MoS$_2$@Li, the polarization curves are stable over time even at higher current densities of 1.6 mA cm^{-2}. Further increase in current densities leads to fluctuations in the polarization curves which show the
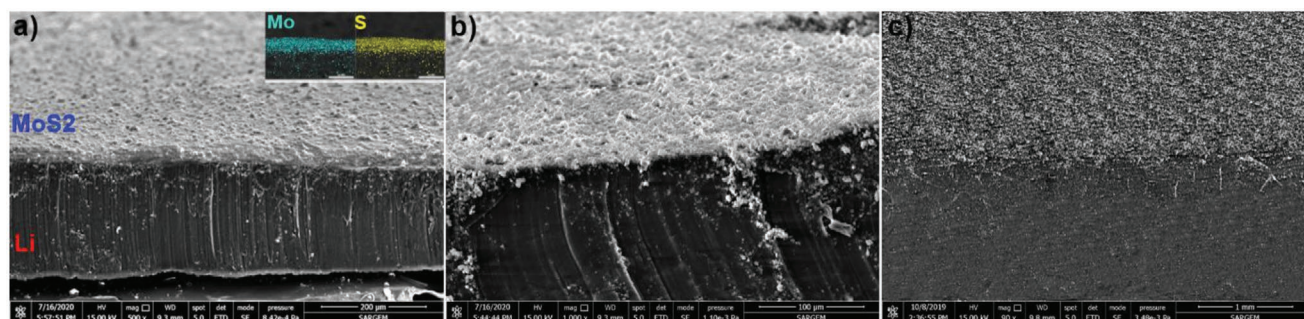

Figure 2. MoS$_2$ layer on lithium chip from cross section a) low magnification with EDS map analysis in the inset, b) high magnification, and c) MoS$_2$ layer on lithium chip surface. (Scale bars: 200 µm, 100 µm and 1 mm for image (a), (b), and (c), respectively).
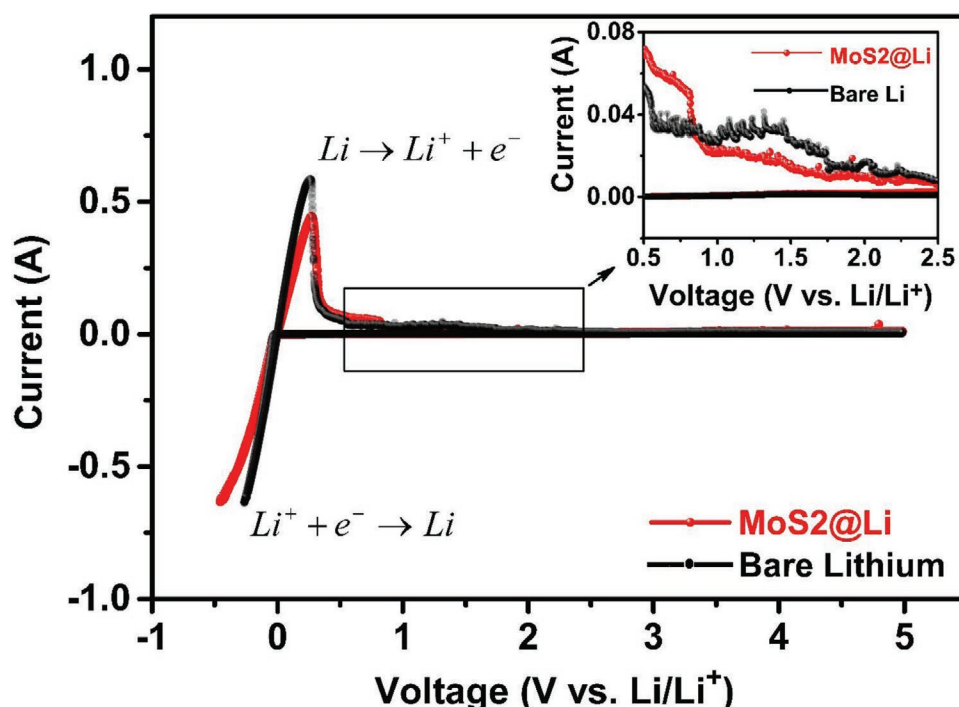
Figure 3. CV analysis of $MoS_2@Li/Li_7P_3S_{11}/SUS$ and $Li/Li_7P_3S_{11}/SUS$ cells.

deterioration of electrode/electrolyte interface in the $MoS_2@Li$ system.

To check the effect of MoS_2 coating on the electrochemical performance of the cell, CV analysis was carried out to characterize electrochemical reactions and corresponding voltages in which the reactions take place. **Figure 5** displays the CV analysis of the batteries in which bare lithium and MoS_2 coated lithium were utilized as an anode. In all-solid-state lithium sulfur batteries, the reactions governing the electrochemical behavior of the cell is known to be different than lithium–sulfur batteries with liquid electrolytes.[50,51] On the cathodic scan, one reduction peak at around 1.75 V was observed which stands for the reduction of S_8 into Li_2S where the corresponding reaction was observed in anodic scan at around 2.4 V which is due to oxidation of Li_2S reverse back into S_8. The overall reaction governing all-solid-state lithium-sulfur batteries was confirmed as

$S + 2Li^+ + 2e^- \leftrightarrow Li_2S$. Besides, the overlap of the curves represents the cyclic stability of the systems. The cell assembled with the $MoS_2@Li$ as anode is expected to preserve the capacity for longer cycles and experience less capacity fade upon cycling.

Galvanostatic charge–discharge tests were conducted at the current density of 0.4 mA cm^{-2} for 200 cycles to test the cycling stability of the cells with and without MoS_2 coating on lithium anode. **Figure 6** displays the cycling profiles of the cells in the voltage range of 1.2–3 V. Cell assembled with MoS_2 coating displays an initial discharge capacity of 675.8 mAh g^{-1} and after 200 cycles capacity fade was measured as 13.58%. However, in the cell assembled with bare lithium anode, the capacity loss after 200 cycles was 27.3%. Our results indicate the stabilization of lithium/$Li_7P_3S_{11}$ interface thorough an artificial MoS_2 layer which prevents the degradation of the solid electrolyte and lithium anode.
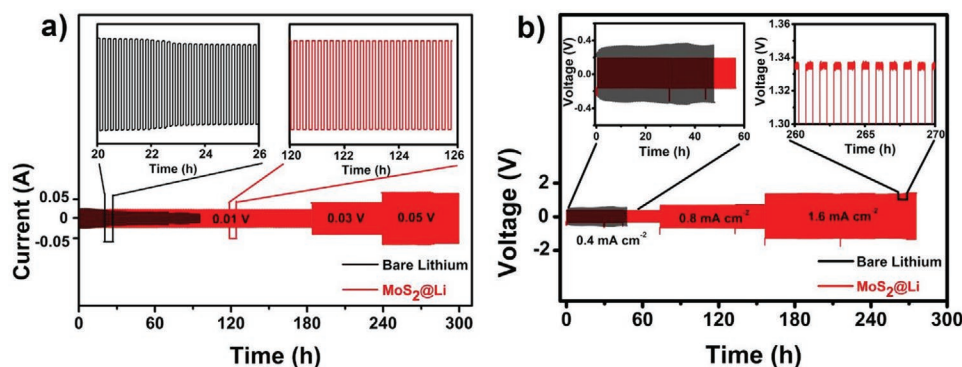

Figure 4. a) Chronoamperometry analysis of symmetric cells assembled with bare lithium and $MoS_2@Li$ as anode at different voltages and b) chrono-voltammetry analysis of symmetric cells assembled with bare lithium and $MoS_2@Li$ as anode at different current densities.
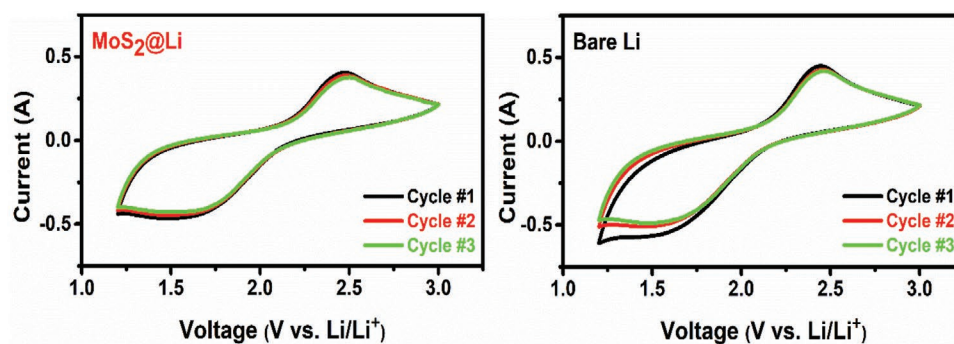
Figure 5. CV analysis of all solid state a) $MoS_2@Li/Li_7P_3S_{11}/S$ and b) $Li/Li_7P_3S_{11}/S$ cells.

Figure 7a displays the discharge capacity of the cells upon cycling. Discharge capacity was shown to more stable in the cell assembled with MoS_2 coating and the capacity loss in the cell with bare lithium anode is evident. The impedance spectra of the cells were measured and the results are shown in Figure 7b. The Nyquist plots for both cells display an incomplete semicircle in the high frequency region and a linear spike at the low frequency region as common in all-solid-state batteries with sulfur based solid electrolytes. The intercept between the real part of the impedance plot and linear spike stands for the total impedance of the cell arising from the charge transfer resistance and interface resistance due to anode–electrolyte contact. Nyquist plots show that the total impedance of the cell is lower in the cell with MoS_2 coating and the increase in the total impedance of the cell is reduced. However, in the cell assembled with a bare lithium anode, the total resistance of the cell increases substantially possibly due to the formation of a layer composed of Li_2S and Li_3P phases as $Li_7P_3S_{11}$ decomposed.[46,52] Continuous increase in the thickness of the SEI layer due to the degradation of solid electrolytes would inevitably increase the total impedance of the cell as evidenced in the cell assembled with bare lithium anode.

3. Conclusion

In summary, lithium anode surface has been modified with MoS_2 via a facile coating route. Noticeably, the electrochemical performance of the cell assembled with MoS_2 layer on the anode surface was increased. The increased electrochemical performance was attributed to the stabilization of the electrode/electrolyte interface as verified by chronoamperometry and chronovoltammetry tests. Besides, the coating layer was also shown to neither prevents the electrochemical reactions of the cell nor increases the total impedance of the cell due to the ionic conductive nature of the layer. By constructing an all-solid-state lithium sulfur battery with MoS_2 coating layer on lithium surface, we have obtained initial and final discharge capacities of 675.8 and 584.1 mAh g^{-1} with 13.58% capacity fade after 200 cycles. Same analysis yields a 27.3% capacity loss in the cell assembled with bare lithium anode. Our results demonstrate the significant effect of solid electrolyte interface on the electrochemical performance of the cell and serve a facile synthesis route to prevent the degradation of anode and electrolyte in all-solid-state batteries by imposing an artificial layer using 2D MoS_2 nanosheets between anode and electrolyte.

4. Experimental Section

Synthesis of solid electrolyte used in this study was reported in the previous study.[10] Phase analysis of MoS_2 coating was carried out by Rigaku D/MAX 2000 type X-ray spectrometer with Cu K_α radiation between 5° and 90° with 1° min^{-1} scan rate. The morphology and elemental mapping of the MoS_2 coating were observed with an FESEM (FEI Quanta FEG 450).

2D MoS_2 was exfoliated using the electrochemical intercalation of Li^+ according to the previous study.[53] Briefly, a MoS_2 pellet prepared from MoS_2 powders used as working electrode, Pt mesh was counter electrode, Ag wire was the reference electrode, and 1M $LiClO_4$ dissolved in ethylene carbonate and dimethyl carbonate mixture (1:1 based on volume) was used as an electrolyte for electrochemical exfoliation process. The electrochemical lithiation process was performed by chronoamperometry technique at −4.5 V potential for 3 h. The Li
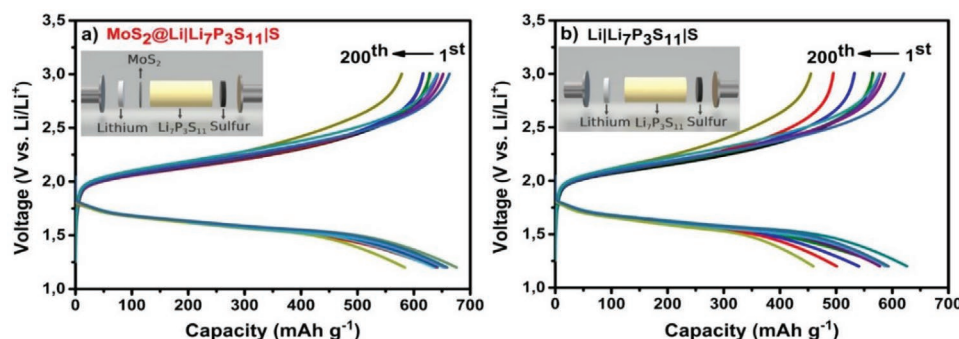

Figure 6. Galvanostatic charge–discharge analysis of all solid state a) $MoS_2@Li/Li_7P_3S_{11}/S$ and b) $Li/Li_7P_3S_{11}/S$ cells.

ADVANCED
SCIENCE NEWS
www.advancedsciencenews.com

ADVANCED
MATERIALS
INTERFACES
www.advmatinterfaces.de

Figure 7. Cycle analysis of all solid state a) MoS_2@Li/$Li_7P_3S_{11}$/S and Li/$Li_7P_3S_{11}$/S cells and, b) Nyquist plots for MoS_2@Li/$Li_7P_3S_{11}$/S and Li/$Li_7P_3S_{11}$/S cells before and after galvanostatic cycling.

intercalated MoS_2 pellet was then immediately immersed into DI water to exfoliate MoS_2 layers while the Li^+ transform into LiOH. The obtained MoS_2 aqueous suspension was first washed with *n*-hexane and then with water to remove organic impurities. Finally, exfoliated 2D MoS_2 product was obtained after filtering the suspension.

Typically, 2 mg exfoliated MoS_2 with 2H structure was then spread onto lithium chip (ø16 mm) and pasted by rubbing with a cotton bar. After a homogeneous layer was obtained, further analysis on the homogeneity of the coating layer was verified by FESEM analysis.

Sulfur based cathode synthesis was carried out by melt-diffusion method. Sublimed sulfur and graphene (4:1 wt%) were initially mixed in an agate mortar and heat treated at 155 °C for 10 h in a sealed glass jar to melt and diffuse sulfur into graphene. Obtained graphene/sulfur composite was then mixed with carbon black and $Li_7P_3S_{11}$ by ball milling for 12 h at 370 rpm. Overall sulfur content in the composite cathode was 36 wt%.

The electrochemical measurements were conducted on all-solid-state PEEK insulated battery cell (ø10 mm). The cell was assembled as follows. 100 mg $Li_7P_3S_{11}$ solid electrolyte was pressed under 340 MPa to obtain a solid electrolyte pellet. 4 mg sulfur based composite cathode powder was then loaded on one side of the pellet and pressed under 240 MPa. Finally, bare lithium or MoS_2 coated lithium chip was attached to the other side of the pellet and pressed under 120 MPa to get the three layered cell. Stainless steel punches of the battery mold acted as a pressure transmitting media along with current collectors in the cell. All process was conducted inside glovebox to prevent the exposure of solid electrolyte to air.

Electrochemical impedance spectroscopy analysis was carried out in the frequency range of 1 Hz–1 MHz at 10 mV AC voltage. CV analysis was conducted in Gamry Ref. 1000 galvanostat between 1.2 and 3 V at a scan rate of 0.5 mV s^{-1}. The galvanostatic charge–discharge tests were carried out between 1.2 and 3 V with a current density of 0.4 mA cm^{-2} at 40 °C. Chronoamperometry analysis was performed in symmetric Li/$Li_7P_3S_{11}$/Li and MoS_2@Li/$Li_7P_3S_{11}$/MoS_2@Li cells at different voltages. Similarly, chronovoltammetry analysis was carried out in symmetric cells at different current densities.

The visualizations of the structures were generated with VESTA.[54]

Conflict of Interest

The authors declare no conflict of interest.

[1] X. Xu, S. Wang, H. Wang, B. Xu, C. Hu, Y. Jin, J. Liu, H. Yan, *J. Energy Storage* **2017**, *13*, 387.

[2] W. Ren, W. Ma, S. Zhang, B. Tang, *Energy Storage Mater.* **2019**, *23*, 707.

[3] S.-K. Lee, Y. J. Lee, Y.-K. Sun, *J. Power Sources* **2016**, *323*, 174.

[4] W. Xu, J. Wang, F. Ding, X. Chen, E. Nasybulin, Y. Zhang, J.-G. Zhang, *Energy Environ. Sci.* **2014**, *7*, 513.

[5] M. S. Kim, Deepika, S. H. Lee, M.-S. Kim, J.-H. Ryu, K.-R. Lee, L. A. Archer, W. Il Cho, *Sci. Adv.* **2019**, *5*, 5587.

[6] N. Kamaya, K. Homma, Y. Yamakawa, M. Hirayama, R. Kanno, M. Yonemura, T. Kamiyama, Y. Kato, S. Hama, K. Kawamoto, A. Mitsui, *Nat. Mater.* **2011**, *10*, 682.

[7] Y. Kato, S. Hori, T. Saito, K. Suzuki, M. Hirayama, A. Mitsui, M. Yonemura, H. Iba, R. Kanno, *Nat. Energy* **2016**, *1*, 16030.

[8] H. Yamane, M. Shibata, Y. Shimane, T. Junke, Y. Seino, S. Adams, K. Minami, A. Hayashi, M. Tatsumisago, *Solid State Ionics* **2007**, *178*, 1163.

[9] Q. Ge, L. Zhou, Y. Lian, X. Zhang, R. Chen, W. Yang, *Electrochem. Commun.* **2018**, *97*, 100.

[10] A. Kızılaslan, H. Akbulut, *ChemPlusChem* **2019**, *84*, 183.

[11] Y. Li, Y. Sun, A. Pei, K. Chen, A. Vailionis, Y. Li, G. Zheng, J. Sun, Y. Cui, *ACS Cent. Sci.* **2018**, *4*, 97.

[12] B. Scrosati, J. Garche, W. Tillmetz, *Advances in Battery Technologies for Electric Vehicles*, 1st ed., Woodhead Publishing, Cambridge **2015**.

[13] H. Xu, Y. Li, A. Zhou, N. Wu, S. Xin, Z. Li, J. B. Goodenough, *Nano Lett.* **2018**, *18*, 7414.

[14] X. Han, Y. Gong, K. (Kelvin) Fu, X. He, G. T. Hitz, J. Dai, A. Pearse, B. Liu, H. Wang, G. Rubloff, Y. Mo, V. Thangadurai, E. D. Wachsman, L. Hu, *Nat. Mater.* **2017**, *16*, 572.

[15] A. Schwöbel, R. Hausbrand, W. Jaegermann, *Solid State Ionics* **2015**, *273*, 51.

[16] Q. Cheng, J. Pang, D. Sun, J. Wang, S. Zhang, F. Liu, Y. Chen, R. Yang, N. Liang, X. Lu, Y. Ji, J. Wang, C. Zhang, Y. Sang, H. Liu, W. Zhou, *InfoMat* **2020**, *2*, 656.

[17] Q. Hao, J. Pang, Y. Zhang, J. Wang, L. Ma, O. G. Schmidt, *Adv. Opt. Mater.* **2018**, *6*, 1700984.

ADVANCED
SCIENCE NEWS

www.advancedsciencenews.com

ADVANCED
MATERIALS
INTERFACES

www.advmatinterfaces.de

[18] Y. Sang, Z. Zhao, M. Zhao, P. Hao, Y. Leng, H. Liu, *Adv. Mater.* **2015**, *27*, 363.

[19] J. Wang, S. Liu, J. Pang, P. Song, W. Tang, Y. Ren, W. Xia, *Appl. Phys. Express* **2020**, *13*, 052004.

[20] S. Jayabal, J. Wu, J. Chen, D. Geng, X. Meng, *Mater. Today Energy* **2018**, *10*, 264.

[21] J. Huang, Z. Wei, J. Liao, W. Ni, C. Wang, J. Ma, *J. Energy Chem.* **2019**, *33*, 100.

[22] D. Chen, W. Chen, L. Ma, G. Ji, K. Chang, J. Y. Lee, *Mater. Today* **2014**, *17*, 184.

[23] A. K. Singh, P. Kumar, D. J. Late, A. Kumar, S. Patel, J. Singh, *Appl. Mater. Today* **2018**, *13*, 242.

[24] H. Wang, D. Tran, J. Qian, F. Ding, D. Losic, *Adv. Mater. Interfaces* **2019**, *6*, 1900915.

[25] Y. Cao, X. Zhu, J. Jiang, C. Liu, J. Zhou, J. Ni, J. Zhang, J. Pang, *Sol. Energy Mater. Sol. Cells* **2020**, *206*, 110279.

[26] W. Liu, J. He, Z. Li, W. Jiang, J. Pang, Y. Zhang, Y. Sun, *Phys. Scr.* **2012**, *85*, 055806.

[27] E. Cha, M. D. Patel, J. Park, J. Hwang, V. Prasad, K. Cho, W. Choi, *Nat. Nanotechnol.* **2018**, *13*, 337.

[28] Y. Li, K. Chang, Z. Sun, E. Shangguan, H. Tang, B. Li, J. Sun, Z. Chang, *ACS Appl. Energy Mater.* **2020**, *3*, 998.

[29] Y. Li, D. Wu, Z. Zhou, C. R. Cabrera, Z. Chen, *J. Phys. Chem. Lett.* **2012**, *3*, 2221.

[30] X. Sun, Z. Wang, *Beilstein J. Nanotechnol.* **2017**, *8*, 2711.

[31] Y. Y. Li, D. Wu, Z. Zhou, C. R. Cabrera, Z. Chen, J. Shuai, H. D. Yoo, Y. Liang, Y. Y. Li, Y. Yao, L. C. Grabow, X. Sun, Z. Wang, Y. Q. Fu, *J. Phys. Chem. Lett.* **2015**, *637*, 1.

[32] H. J. Chen, J. Huang, X. L. Lei, M. S. Wu, G. Liu, C. Y. Ouyang, B. Xu, *Int. J. Electrochem. Sci.* **2013**, *8*, 2196.

[33] L. David, R. Bhandavat, G. Singh, *ACS Nano* **2014**, *8*, 1759.

[34] J. Shuai, H. D. Yoo, Y. Liang, Y. Li, Y. Yao, L. C. Grabow, *Mater. Res. Express* **2016**, *3*, 064001.

[35] K. Qi, Z. Yuan, Y. Hou, R. Zhao, B. Zhang, *Appl. Surf. Sci.* **2019**, *483*, 688.

[36] H. Xue, S. Yue, J. Wang, Y. Zhao, Q. Li, M. Yin, S. Wang, C. Feng, Q. Wu, H. Li, D. Shi, Q. Jiao, *J. Electroanal. Chem.* **2019**, *840*, 230.

[37] J. Wang, L. Zhang, K. Sun, J. He, Y. Zheng, C. Xu, Y. Zhang, Y. Chen, M. Li, *Chem. Eng. J.* **2019**, *372*, 665.

[38] W. Hirunpinyopas, E. Prestat, P. Iamprasertkun, M. A. Bissett, R. A. W. Dryfe, *2D Mater.* **2020**, *7*, 015030.

[39] M. Deng, K. Kwac, M. Li, Y. Jung, H. G. Park, *Nano Lett.* **2017**, *17*, 2342.

[40] Z. A. Ghazi, X. He, A. M. Khattak, N. A. Khan, B. Liang, A. Iqbal, J. Wang, H. Sin, L. Li, Z. Tang, *Adv. Mater.* **2017**, *29*, 1606817.

[41] L. Ries, E. Petit, T. Michel, C. C. Diogo, C. Gervais, C. Salameh, M. Bechelany, S. Balme, P. Miele, N. Onofrio, D. Voiry, *Nat. Mater.* **2019**, *18*, 1112.

[42] E. Cha, M. D. Patel, J. Park, J. Hwang, V. Prasad, K. Cho, W. Choi, *Nat. Nanotechnol.* **2018**, *13*, 337.

[43] X. Yao, D. Liu, C. Wang, P. Long, G. Peng, Y.-S. Hu, H. Li, L. Chen, X. Xu, *Nano Lett.* **2016**, *16*, 7148.

[44] R. Xu, X. Xia, X. Wang, Y. Xia, J. Tu, *J. Mater. Chem. A* **2017**, *5*, 2829.

[45] Z. Shen, W. Zhang, G. Zhu, Y. Huang, Q. Feng, Y. Lu, *Small Methods* **2020**, *4*, 1900592.

[46] S. Wenzel, T. Leichtweiss, D. Krüger, J. Sann, D. Krüger, J. Sann, J. J. Janek, *Solid State Ionics* **2015**, *278*, 98.

[47] S. Wenzel, S. Randau, T. Leichtweiß, D. A. Weber, J. Sann, W. G. Zeier, J. Janek, *Chem. Mater.* **2016**, *28*, 2400.

[48] X.-B. Cheng, C. Yan, H.-J. Peng, J.-Q. Huang, S.-T. Yang, Q. Zhang, *Energy Storage Mater.* **2018**, *10*, 199.

[49] Y. Tian, T. Shi, W. D. Richards, J. Li, J. C. Kim, S. H. Bo, G. Ceder, *Energy Environ. Sci.* **2017**, *10*, 1150.

[50] Q. Zhang, N. Huang, Z. Huang, L. Cai, J. Wu, X. Yao, *J. Energy Chem.* **2020**, *40*, 151.

[51] X. Yao, N. Huang, F. Han, Q. Zhang, H. Wan, J. P. Mwizerwa, C. Wang, X. Xu, *Adv. Energy Mater.* **2017**, *7*, 1602923.

[52] Q. Zhang, D. Cao, Y. Ma, A. Natan, P. Aurora, H. Zhu, *Adv. Mater.* **2019**, *31*, 1901131.

[53] A. Ejigu, I. A. Kinloch, E. Prestat, R. A. W. Dryfe, *J. Mater. Chem. A* **2017**, *5*, 11316.

[54] K. Momma, F. Izumi, *J. Appl. Crystallogr.* **2011**, *44*, 1272.

2001020 (7 of 7)